JACS
JOURNAL OF THE AMERICAN CHEMICAL SOCIETY
Article
pubs.acs.org/JACS

PNA-Peptide Assembly in a 3D DNA Nanocage at Room Temperature

Justin D. Flory,[†,‡] Sandip Shinde,[†,‡] Su Lin,[‡,§] Yan Liu,[†,‡,§] Hao Yan,[†,‡,§] Giovanna Ghirlanda,[†,‡] and Petra Fromme*[,†,‡]

[†]Center for Bio-Inspired Solar Fuel Production, [‡]Department of Chemistry and Biochemistry, and [§]The Biodesign Institute, Arizona State University, Tempe, Arizona 85287, United States

Supporting Information

ABSTRACT: Proteins and peptides fold into dynamic structures that access a broad functional landscape; however, designing artificial polypeptide systems is still a great challenge. Conversely, DNA engineering is now routinely used to build a wide variety of 2D and 3D nanostructures from hybridization based rules, and their functional diversity can be significantly expanded through site specific incorporation of the appropriate guest molecules. Here we demonstrate a new approach to rationally design 3D nucleic acid−amino acid complexes using peptide nucleic acid (PNA) to assemble peptides inside a 3D DNA nanocage. The PNA-peptides were found to bind to the preassembled DNA nanocage in 5−10 min at room temperature, and assembly could be performed in a stepwise fashion. Biophysical characterization of the DNA-PNA-peptide complex was performed using gel electrophoresis as well as steady state and time-resolved fluorescence spectroscopy. Based on these results we have developed a model for the arrangement of the PNA-peptides inside the DNA nanocage. This work demonstrates a flexible new approach to leverage rationally designed nucleic acid (DNA-PNA) nanoscaffolds to guide polypeptide engineering.

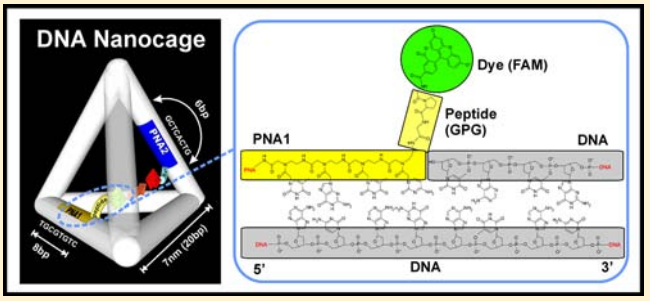

INTRODUCTION

The field of structural DNA nanotechnology has transformed our thinking about the purpose and possibilities of canonical base pairing biopolymers, which can have a much broader structural landscape than what has evolved in natural organisms. The sequences of multiple DNA strands have been designed and assembled into a wide variety of interesting nanostructures, such as a 2D crystal lattice,[1] 3D tetrahedron,[2] 3D crystal,[3] octahedron,[4] various fully addressable 2D nanoscaffolds,[5] and complex 3D shapes.[6] We refer the reader to several excellent reviews of the progress made in this dynamic field and challenges that remain.[7−9]

Because the functional diversity of unmodified DNA is limited, much effort has been focused on introducing functional groups. DNA scaffolds offer a flexible, biocompatible workbench to explore the wide variety of functions performed by proteins in nature, such as catalysis, scaffolding, molecular transport and molecular recognition among others. For example, DNA scaffolds have been used to organize proteins on 2D arrays,[10] to study antibody recognition of peptide epitopes[11] and to investigate the spatial dependence of enzyme cascades.[12] Remarkably nearly all of the biomolecules found in the biosphere are synthesized through unique metabolic pathways of reactions catalyzed by proteins. Some large proteins, such as the 350 kDa protein Photosystem II (PSII), perform multiple functions including light absorption, photochemical conversion, electron transfer, and catalytic water oxidation.[13] While light absorption and most of the electron transfer reaction take place in the membrane intrinsic part of PSII, the catalytic site for water oxidation is located in the membrane extrinsic part of PSII, suggesting that a water-soluble version of the water splitting complex is possible. The crystal structure of PSII[13] shows that coordinating sphere around the metal cluster in the active site is only a small part of the protein, but that the amino acid ligands come from multiple protein subunits. We hypothesize that the scaffolding function of a protein could be replaced by strategically attaching peptides inside the well-defined cavity of a 3D nucleic acid nanoscaffold, which matches the size of the first and second coordination sphere of the catalytic center (<10 nm).

Different bio-orthogonal linking chemistries are required to control peptide assembly within a highly interconnected nucleic acid-polypeptide complex. Erben et al. coupled the protein cytochrome c to one of the strands of the same DNA tetrahedron used in our design and annealed the DNA−protein complex in one step.[14] While this strategy allows the same bio-orthogonal linking chemistry to be used on multiple DNA strands, it requires that all components be assembled at once and under conditions that favor proper DNA nanocage assembly, namely, low concentration (sub micromolar) and high-temperature annealing (optimally 90 °C ramped to room temperature). An alternative linking strategy that allows more control over the assembly process is to use nucleobase hybridization, where the nucleobase sequence is used to provide orthogonal attachment. This approach is routinely used to functionalize large DNA nanostructures, such as DNA origami,[15] because functionaliza-

Received: January 22, 2013
Published: March 25, 2013

   dx.doi.org/10.1021/ja400762c | J. Am. Chem. Soc. 2013, 135, 6985−6993

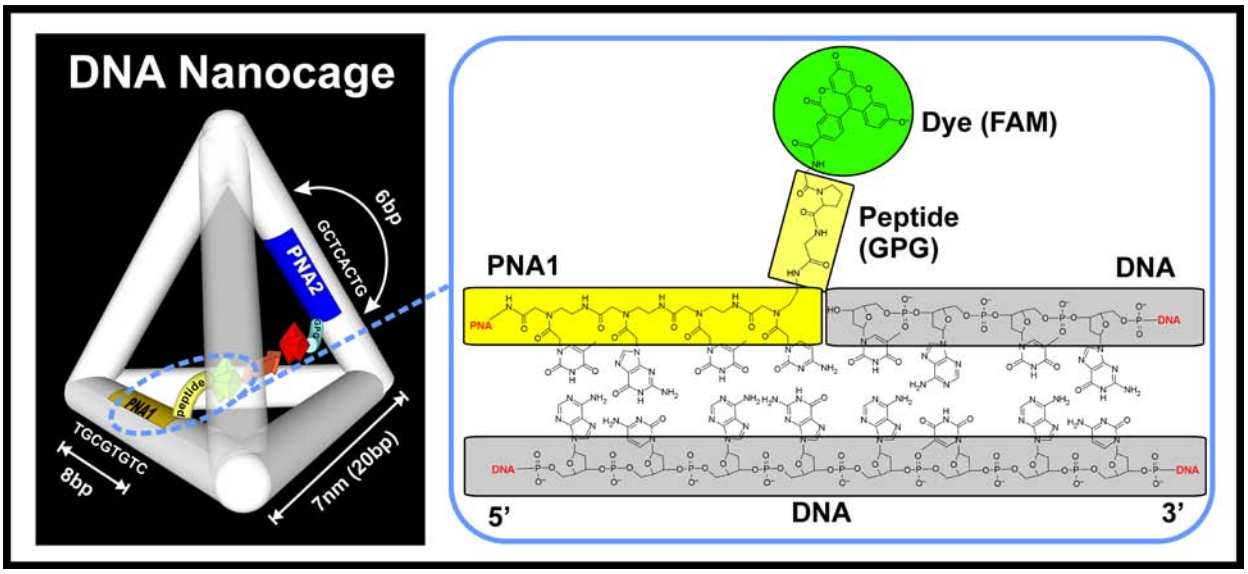

Figure 1. Schematic of the designed dye labeled DNA-PNA-peptide complex. (Left) Cartoon of the proposed design for assembling two fluorescently labeled peptides into a DNA nanocage each using a PNA linker with the indicated sequences. The arrow indicates the direction of energy transfer between the fluorescein (FAM) donor and the tetramethylrhodamine (TMR) acceptor dyes. (Right) Close up showing the chemical structures of the N-terminal (5′) end of the dye labeled PNA1-peptide, the 3′-end of the adjacent DNA strand and the complementary DNA strand that drives the assembly of this peptide into the DNA nanocage. Chemical structures were drawn using Marvin Sketch.[16]

tion can be done after the DNA nanostructure is formed. To allow for sufficient thermal stability at room temperature, typical DNA hybridization linker sequences are at least 15−20 nucleotides (nt) long, which form 4.9−6.5 nm long dsDNA helices upon hybridization. However, such long linker sequences put significant constraints on how the linker can be used in small DNA nanostructures (radius <4 nm). The linker length could be shortened by increasing the GC content of the sequence; however this would limit the sequence variability needed to attach multiple peptides to the DNA nanostructure.

Our approach, as shown in the schematic in Figure 1, is to connect peptides to the DNA scaffold using short (8nt) linker sequences of the more thermostable peptide nucleic acid (PNA) originally developed by Nielsen and co-workers.[17] PNA synthesis is compatible with peptide synthesis, so the polypeptides can be synthesized directly with the linking PNA sequences using established protocols.[18] There is a great interest in using PNA for gene targeting[19] and sensing[20,21] applications because of PNA hypersensitivity to sequence mismatches,[22] its ability to invade double stranded DNA sequences,[17] and its resistance to enzymatic degradation.[23] PNA has also been investigated as a nanoscaffold. First it was incorporated into a two-dimensional DNA array, resulting in only a slight unwinding of the helix[24] and more recently used to arrange peptide ligands along a linear strand of DNA to assemble several protein subunits.[25]

Here we report results for a design strategy using PNA to assemble peptides inside a 3D DNA nanostructure. Two fluorescently labeled PNA-peptides were synthesized using microwave-assisted solid phase synthesis. The PNA-peptides were assembled into the DNA nanostructure in 5−10 min at room temperature. The peptides can be either assembled together or in a specified order. Steady state fluorescence was used to monitor Förster resonance energy transfer (FRET) between a single dye labeled PNA-peptide bound to the DNA nanocage with a complementary dye label, in order to determine the temperature of PNA dissociation out of the DNA nanocage. Time-resolved fluorescence spectroscopy was used to identify different interactions and decay pathways experienced by each fluorescent dye in the DNA-PNA-peptide complex. Finally, FRET theory was used to calculate the distances between the two PNA-peptides bound to the DNA nanocage and build a model of the designed complex. In the future this design principle could lead to the assembly of enzyme active centers inside DNA nanocages.

RESULTS AND DISCUSSION

DNA-PNA-Peptide Complex Design. Our design is based on a DNA tetrahedron assembled out of four 63nt ssDNA sequences originally designed by Goodman and co-workers.[2] The sequences of each strand are unique and fully addressable for incorporating guest molecules through hybridization based linkers such as PNA (Figure S1). The authors were able to identify the location of the major and minor grooves and approximate base orientations through a series of DNA linking[2] and protein encapsulation experiments,[14] along with electron density from cryo-electron microscopy.[26] We inferred from their study that base positions around the 8th and 18th bases point inward and around the 3rd and 14th base point outward when counting from the vertex in the 3′-direction. We introduced an 8nt single stranded gap in the center of opposite 20 base pair (bp) edges of the DNA nanocage to bind two PNA strands each containing a short prototype peptide (Gly-Pro-Gly) protruding from the N-terminus (5′) of the PNA sequence into the DNA nanocage at the 7th base position (Figure 1). Because of the structural symmetry of the DNA nanocage, the same strategy can be applied to any edge in the DNA nanocage, thereby allowing a number of different peptides to be assembled at sequence specific locations. The 8nt length of each PNA binding domain was chosen to provide sufficient thermal stability of PNA binding to the DNA nanocage with minimal disruption of the DNA nanocage structure in the absence of the PNA-peptide. Standard dsDNA of B-DNA form has a helical pitch of 10.5 bp/turn,[27,28] whereas PNA-DNA duplexes have been observed to adopt a helical pitch from 13.0 bp/turn[29] to 15.6 bp/turn.[24] For the 8bp

dx.doi.org/10.1021/ja400762c | J. Am. Chem. Soc. 2013, 135, 6985−6993

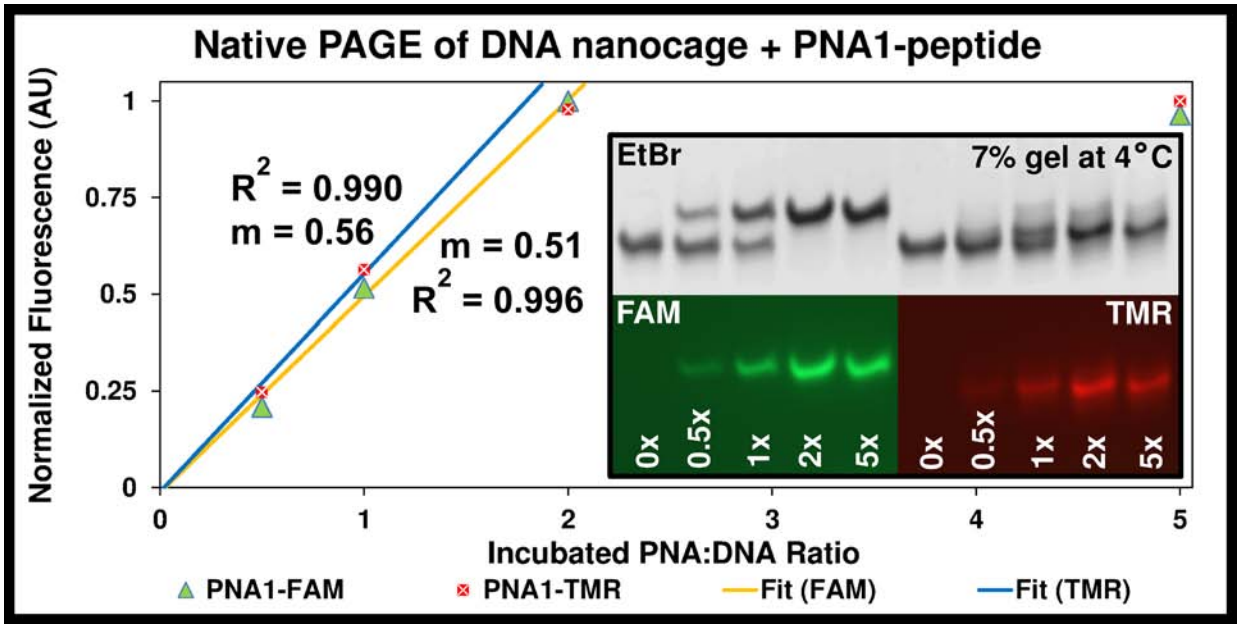

Figure 2. Native PAGE of the DNA nanocage hybridized to increasing molar excess of the PNA1-peptide labeled with the fluorescent dyes FAM and TMR. The DNA nanocage was incubated at room temperature for 5−10 min with increasing molar excess of PNA1-peptide labeled with TMR and with FAM. The upper image shows EtBr fluorescence (Ex. 302 nm, Em. 605 nm) after staining, while the lower images were taken of the native dye fluorescence (FAM Ex. 475 nm, Em. 535 nm; TMR Ex. 560 nm, Em. 645 nm) prior to EtBr staining. The normalized integrated fluorescence intensities of the gel bands are shown plotted versus the incubated PNA to DNA ratio, where the initial hybridization fit a linear model. The slope *m* represents the fraction of PNA that binds to the DNA nanocage.

PNA-DNA domain in our design this leads to an underwinding of the helix by 53−90°, respectively, along the edges that bind PNA. However, the original DNA nanocage design[2] included unhybridized adenosine nucleotides connecting each edge of the DNA nanocage,which should be able to counter rotate and neutralize this effect. Throughout this report we use the nomenclature defined in Figures S1 and S2 when we describe the various strands and constructs used in each experiment. Briefly, PNA1 (TGCGTGTC) and PNA2 (GCTCACTG) are both PNA sequences written from C to N (3′ to 5′), abbreviated as PNA1 and PNA2, respectively; GPG (Gly-Pro-Gly) is the peptide sequence, and FAM (fluorescein) and TMR (tetramethylrhodamine) are the dye labels.

PNA-Peptide Synthesis and Assembly with the DNA Nanocage. We synthesized two dye labeled PNA-peptides, PNA1-GPG-FAM and PNA2-GPG-TMR, using microwave-assisted solid phase synthesis following established protocols[18,30,31] with some modifications detailed in the Supporting Information, Materials and Methods section. Unlabeled versions of each PNA-peptide were also prepared to serve as controls for fluorescence experiments by acetylating the N terminus. The PNA-peptide constructs were purified using reverse-phase high pressure liquid chromatography (RP-HPLC) and identified using matrix-assisted laser desorption−ionization (MALDI) mass spectrometry. MALDI and RP-HPLC chromatograms are shown for all products in Figures S3 and S4, respectively.

PNA-DNA duplexes are typically formed from single stranded DNA and PNA by heating both strands to around 90 °C to remove any secondary structure or sample aggregation, followed by cooling to room temperature or below.[32] Alternatively, short PNA sequences have been shown to bind to their target DNA sequence after incubating for 5−10 min at room temperature.[33] This incubation strategy is especially important for hybridizing PNA-peptides to 3D DNA nanostructures, because assembling peptides inside a preformed DNA nanocage avoids the high temperature annealing step, which could denature the polypeptide structure. Furthermore the incubation strategy allows for higher PNA-peptide concentrations to drive more rapid assembly and lets the PNA-peptides be assembled in a desired order.

In order to determine the PNA-peptide hybridization efficiency, the DNA nanocage was prepared (without any PNA) by annealing and purified by size-exclusion high-pressure liquid chromatography (SE-HPLC), as shown in Figure S5A. The preformed DNA nanocage was incubated for 5−10 min at room temperature with increasing molar excess (0*x* to 5*x*) of PNA1-GPG labeled with FAM and separately with PNA1-GPG labeled with TMR. The samples were cooled to 4 °C and were directly analyzed using native polyacrylamide gel electrophoresis (PAGE) at 4 °C. The bands of interest are shown in Figure 2, and the complete gel is shown in Figure S6. Both constructs exhibit a band shift upon PNA binding which could be due in part to the DNA nanocage becoming less spherical and more tetrahedral in shape with a slightly larger diameter after PNA binding. PNA1-GPG-FAM shows the most dramatic shift, which could be further enhanced from the FAM^{2-} dianion being repelled away from the negatively charged DNA nanocage, forcing the attached peptide to adopt an orientation pointing outward and further retarding migration of the complex through the gel. The chemical structures of FAM and TMR are shown in Figure S7.

The gel in Figure 2 also shows that PNA1-GPG-TMR induces some structural heterogeneity upon binding. In addition to a distinct band showing TMR fluorescence, some minor band broadening is apparent that extends from the initial position of DNA nanocage without any PNA up to the PNA1-GPG-FAM band, suggesting the TMR peptide stabilizes a range of slightly different DNA nanocage conformations. Figure 2 also shows the ratio of PNA bound to the DNA nanocage calculated from the

dx.doi.org/10.1021/ja400762c | J. Am. Chem. Soc. 2013, 135, 6985−6993

integrated band intensities, which increases linearly with the added molar excess until saturation is achieved by two times excess. The PNA1-GPG hybridization was further confirmed using absorption spectroscopy by comparing the absorption of the dye labeled PNA to that of the DNA nanocage after removing the unhybridized PNA. The PNA-peptide hybridization increases linearly until PNA-peptide saturation occurs just after two times excess for PNA1-GPG-TMR (extrapolated to 2.4x) and for PNA1-GPG-FAM (extrapolated to 2.5x), as shown in Figure S8.

The need for excess PNA-peptide to achieve quantitative binding to the DNA nanocage is likely because a fraction of the PNA-peptides irreversibly self-aggregate before binding to the DNA nanocage. Some PNA sequences show mild aggregation at concentrations as low as 1 μM and are often modified to improve solubility.[34] However, once bound to the DNA nanocage, the PNA-peptides are quite stable at low temperatures, even once excess PNA-peptides are removed. To ensure quantitative PNA-peptide binding to the DNA nanocage, five times molar excess was used to prepare the constructs for all subsequent experiments. Samples were stored at −20 or 4 °C, and experiments were carried out between 4 and 11 °C to prevent PNA-peptide dissociation.

A time course study was performed in order to determine the kinetics of PNA hybridization to the 3D DNA nanocage. Fluorescently labeled DNA nanocages were prepared using one strand labeled by the manufacturer (Integrated DNA Technologies) with a dye complementary to that on the PNA-peptide and located at the vertex adjacent to the PNA-peptide's N-terminus. The fluorescence intensity of the FAM labeled DNA nanocage (DNA-FAM) was monitored as a function of time after mixing in five times molar excess PNA1-GPG-TMR (PNA1-TMR) with the DNA nanocage at 25 °C, as shown in Figure S10A The data from Figure S10A were converted to the fraction of PNA-peptide bound as described in the Supporting Information, Materials and Methods section, and plotted in Figure S10B. 86% of the PNA bound while mixing the PNA during the first 15 s, 94% after 1 min and 99% after 5 min. Such rapid hybridization of short PNA sequences to DNA is in agreement with another kinetic study of PNA-DNA duplex formation.[33]

DNA nanocages were also prepared with both dye-labeled PNA-peptides for fluorescence characterization. Five times molar excess of the each PNA-peptide was incubated at room temperature for 5−10 min and with the preformed DNA nanocage, then chilled on ice for 1 h. The unhybridized PNA-peptides were removed by SE-HPLC with the column cooled to 4 °C. The chromatogram of the fully assembled DNA nanocage with both dye labeled PNA-peptides (DNA + PNA1-FAM + PNA2-TMR) is shown in Figure S5B. The PNA-peptides could also be assembled in stepwise fashion by first forming the DNA nanocage with one PNA-peptide, removing excess PNA-peptide using 30k MWCO centrifugal filters, adding the second PNA-peptide and removing excess PNA-peptide in the same fashion. This strategy produced the same end product as when both PNA-peptides were assembled simultaneously (data not shown).

DNA-PNA-Peptide Thermal Stability. We quantified the thermal stability of PNA1-GPG when labeled with each dye and bound to the DNA nanocage by incubating PNA1-GPG-TMR and PNA1-GPG-FAM with DNA nanocages labeled with the complementary dye at the vertex adjacent to the PNA-peptide (e.g., DNA-FAM and DNA-TMR, respectively), as shown in complexes A and B at the bottom of Figure 3. The top and middle figures in Figure 3 show the fluorescence spectra taken of the complex DNA-FAM + PNA1-TMR and DNA-TMR + PNA1-FAM, respectively, as defined in Figure S2, while gradually heated

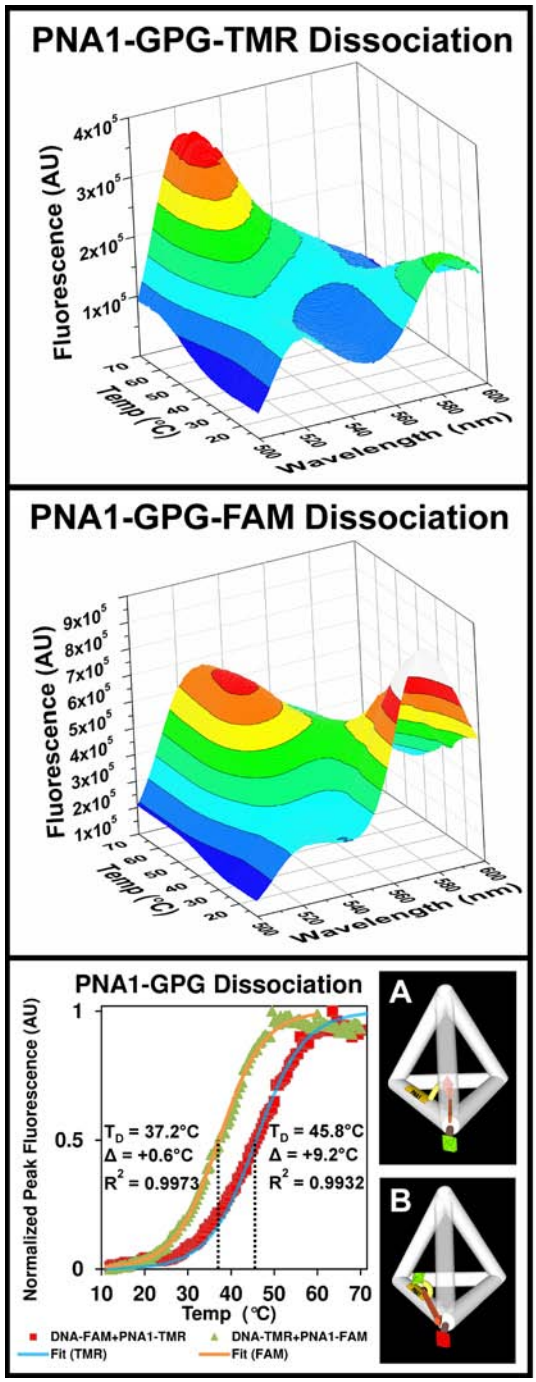

Figure 3. Fluorescence spectra of the TMR and FAM labeled PNA1-peptide bound to the FAM and TMR labeled DNA nanocage as a function of temperature. (Top) PNA1-GPG labeled with TMR bound to the DNA nanocage labeled with FAM (DNA-FAM + PNA1-TMR), as shown in schematic "A" of the bottom figure. (Middle) PNA1-GPG labeled with FAM bound to the DNA nanocage labeled with TMR (DNA-TMR + PNA1-FAM), as shown in schematic "B" of the bottom figure. (Bottom) The peak donor fluorescence is plotted versus temperature and fitted with a sigmoidal dose response curve, where the inflection point corresponds to the T_D indicated on the plot. The difference (Δ) from a theoretical value (36.6 °C) is also shown, which is greater than that predicted for a similar DNA sequence (34.5 °C).

dx.doi.org/10.1021/ja400762c | J. Am. Chem. Soc. 2013, 135, 6985−6993

from 11 to 85 °C. Initially for both complexes, the donor (FAM) fluorescence is significantly quenched because FRET occurs when the complex is fully assembled with the donor and acceptor in close proximity. As the temperature increases and the PNA-peptide dissociates from the DNA nanocage, the FRET signal becomes negligible as the separation between the donor and acceptor becomes large causing the donor fluorescence to increase significantly.

The change in peak donor fluorescence with temperature in the presence of the acceptor was corrected for the change in fluorescence of the donor alone with temperature (Figure S9) and was fitted with a sigmoidal dose response curve (Figure 3, bottom), where the inflection point of the fitted curve indicates the dissociation temperature (T_D) of the PNA-peptide from the DNA nanocage. We use the term T_D instead of melting temperature (T_m) to avoid confusion from the melting of the DNA nanocage itself, which occurs at temperatures (~60 °C) above the dissociation of the PNA-peptides from the DNA nanocage.[35] We then used a method described by Giesen and co-workers[36] to predict the T_D of a PNA-DNA duplexes based on the T_D of a DNA−DNA duplex with the same sequence, the length of the sequence and the fraction of pyrimidine bases also shown in Figure 3 (bottom). One possible interpretation of the higher T_D for PNA1-GPG-TMR might be that TMR interacts with guanine residues through π-stacking[37] which could significantly stabilize PNA binding to the DNA nanocage.

While the stability of a DNA-PNA duplex depends on GC content, Sen and Nielsen showed that PNA strands have a much stronger increase in binding enthalpy and free energy with increasing purine content in the PNA strand than a DNA strand with the same sequence, possibly because of structural changes that were too subtle for them to detect by circular dichroism.[38] They demonstrated that a 10mer PNA sequence with 80% purine content increased the T_D to a complementary DNA sequence over a similar DNA sequence by 28.8 °C from 36.2 to 65.0 °C, whereas a 10mer PNA sequence with 80% pyrimidine content only increased the T_D by 2.8 to 39.0 °C. For applications that require higher PNA-peptide binding stability the purine content of our sequences could be increased further.

Fluorescence Characterization: Lifetime, Anisotropy, and Energy Transfer. We used time-correlated single photon counting (TCSPC) to measure the time-resolved fluorescence decay of the dye labels to investigate the degree of interaction between both dye labeled PNA-peptides assembled into the DNA nanocage. Unlabeled PNA-peptides were prepared with N terminal acetylation (Ac) to serve as controls for our fluorescence experiments. The fluorescence decay kinetics of the donor alone (DNA + PNA1-FAM + PNA2-Ac) and the acceptor alone (DNA + PNA1-Ac + PNA2-TMR) were measured at their corresponding fluorescence maxima, and the fluorescence decay kinetics of the donor in the presence of the acceptor (DNA + PNA1-FAM + PNA2-TMR) was measured in the donor-only emission region as shown in Figure 4A. The sequences and strand names of these complexes are defined in Figures S1 and S2, respectively. Exponential fitting of each fluorescence decay required either two or three parameters, which are shown in Table S1. The long-lived component is from the natural decay of each fluorophore. The short-lived component is likely from fluorophore interactions with the DNA nanocage, such as quenching by nearby guanine nucleobases.[39] The medium length component identified for the donor in the presence of the acceptor is likely from energy transfer from donor to acceptor. For each decay the fitted

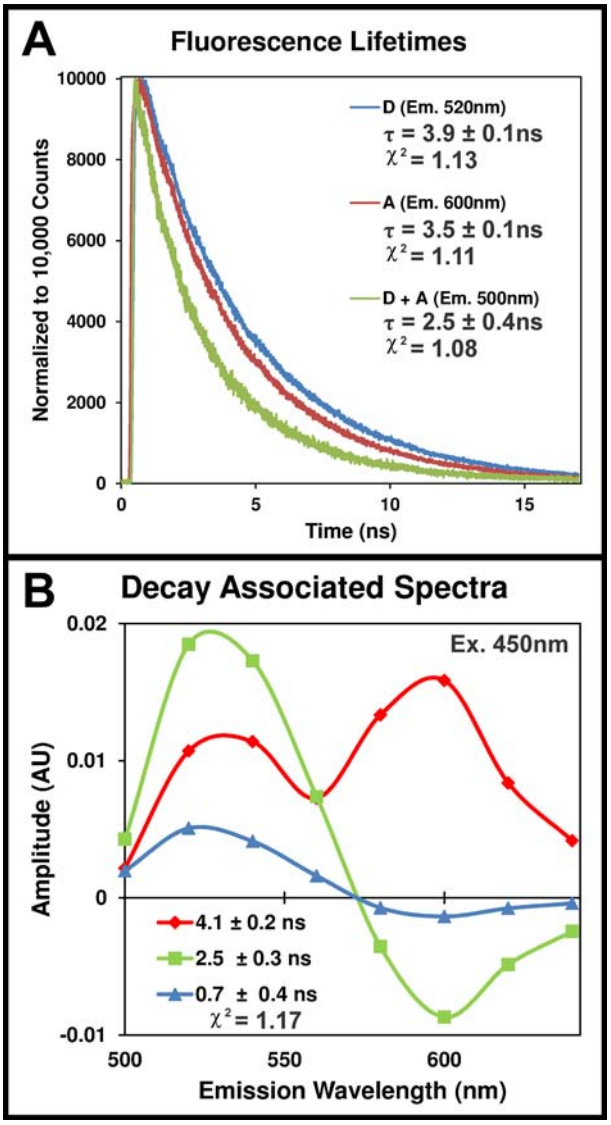

Figure 4. Fluorescence decay of the DNA nanocage with two fluorescently labeled PNA-peptides. (A) Plot of the fluorescence decay kinetics measured by TCSPC at 11 °C of the DNA nanocage with both PNA-peptides labeled with the donor (FAM) only (blue), the acceptor (TMR) only (red) ,and labeled with both the donor and acceptor and detected in the donor only emission region (green). (B) Fluorescence decay spectra were collected at several wavelengths and fit simultaneously to three components using global analysis. The relative amplitudes of each component from the analysis are plotted as a function of wavelength in the decay associated spectra (DAS).

components were averaged to facilitate comparing with the steady state fluorescence data discussed later. The calculated average lifetime of the donor alone is 3.9 ± 0.1 ns, which is in good agreement with another study,[40] as is the calculated average lifetime of the acceptor alone of 3.5 ± 0.1 ns.[37] The average donor lifetime is reduced to 2.5 ± 0.4 ns in the presence of the acceptor due to energy transfer from donor to acceptor, which corresponds to an energy transfer efficiency of 36%.

To gain insight into the different decay pathways of the donor excited state energy, we collected fluorescence decay kinetics data at several wavelengths spanning the donor and acceptor emission spectra. The kinetics curves at all recorded wavelengths were fit simultaneously to three components of the donor−acceptor system using global analysis. The relative amplitudes of

dx.doi.org/10.1021/ja400762c | J. Am. Chem. Soc. 2013, 135, 6985−6993

each component from the analysis are plotted as a function of wavelength in the decay associated spectra (DAS) as shown in Figure 4B. The most dominant component of donor decay has a lifetime of 2.5 ± 0.3 ns and shows a positive peak in the donor emission wavelength region (fluorescence decay) and a similarly sized negative peak (increase in fluorescence) in the acceptor region, which is characteristic of energy transfer from the donor to the acceptor. The second major component has a lifetime of 4.1 ± 0.2 ns, which has a positive peak in both the donor and acceptor region. This component indicates that there is a subpopulation of the donor that does not undergo energy transfer, but instead decays with its natural lifetime, possibly from an orthogonal orientation with respect to the acceptor. Global analysis is unable to resolve the differences in this component from the natural decay of the acceptor and thus provides an average lifetime of both components. The remaining component has a lifetime of 0.7 ± 0.4 ns with a positive peak in the donor region and small negative peak in the acceptor region, suggesting that a second faster pathway for energy transfer exists. The DAS shows energy transfer between both dye labeled PNA-peptides, indicative of proper complex assembly, and suggests that on average the dye labeled peptides adopt two distinct conformational states.

TCSPC was also used to evaluate how freely the dye labels can rotate within the DNA-PNA-peptide complex by probing the rate of depolarization of their emission when excited by polarized light as a function of time. The complex with the acceptor alone (DNA + PNA1-Ac + PNA2-TMR) was excited by vertically polarized light at 500 nm, and the TMR emission was monitored at 600 nm with polarization both parallel (VV, vertical excitation and emission) and perpendicular (VH, vertical excitation and horizontal emission) relative to the polarization of the excitation, as shown in Figure 5A. The difference in the emission intensity of VV and VH was used to determine the anisotropy using the equations described in the Supporting Information, Materials and Methods section. The calculated anisotropy is plotted as a function of time in Figure 5A, which shows a steady decrease in anisotropy from 0.36 initially to 0.24 after 17 ns. The maximum possible anisotropy value is 0.4 for a perfectly rigid complex with no depolarization, whereas the minimum value of zero indicates a rapidly rotating dye molecule that has fully depolarized. This measured value of 0.24 is in excellent agreement with a value (0.24) reported for the steady state anisotropy of a TMR labeled oligonucleotide, due to restricted dye mobility from π stacking with nearby guanine nucleobases.[37] The same method was used to determine the anisotropy of the DNA nanocage directly labeled with TMR (DNA-TMR). Interestingly, the calculated anisotropy of DNA-TMR decays in a nearly identical fashion over time to a value of 0.24 after 17 ns, as shown in Figure 5A. Evidently the TMR dye interacts equally with guanine when intercalated in the DNA helix along the edge or when stacked to one of the terminal guanines at the end of the three helices that converge at the vertex, as identified in the DNA sequences in Figure S1.

The complex with the donor alone (DNA + PNA1-FAM + PNA2-Ac) was measured in the same way as for TMR; however, the sample was excited at 450 nm, and the FAM emission was monitored at 520 nm. The calculated FAM anisotropy decays much faster to a value of 0.12 after 17 ns, as shown in Figure 5B. This value is slightly higher than the steady state values reported in the literature[37] for FAM labeled oligonucleotides, which may be due to the 3D conformation of the DNA nanocage used in our study further restricting the motion of the dye. The calculated

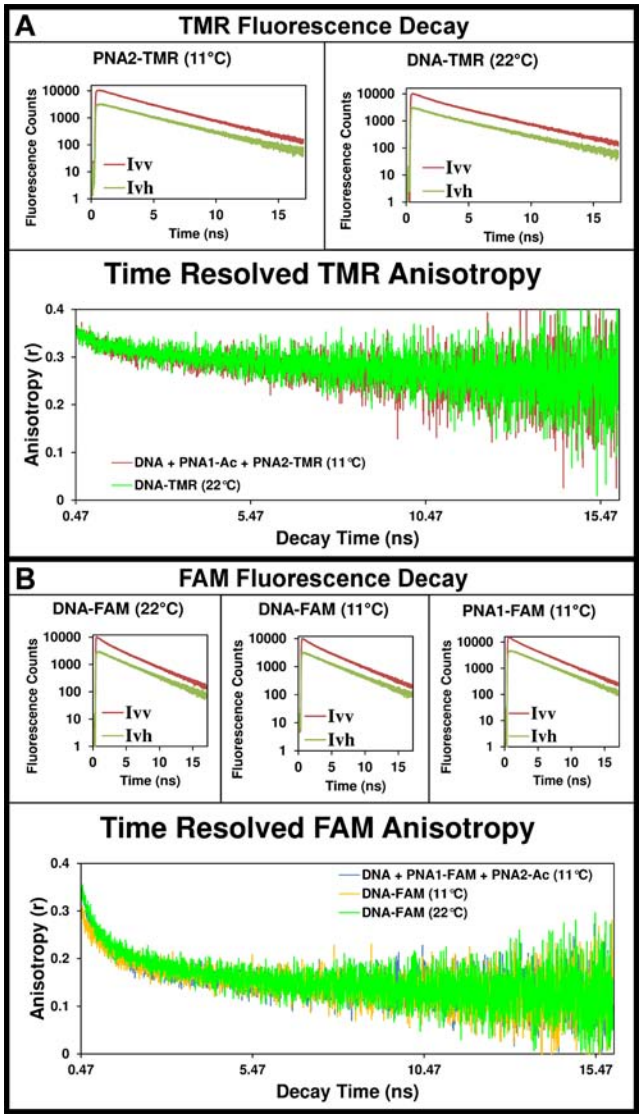

Figure 5. Fluorescence decay and anisotropy of FAM and TMR dyes attached to a complex of a PNA-peptide inside the DNA nanocage. (Top of A and B) Plot of the fluorescence decay of TMR at 600 nm when excited at 500 nm (A) and FAM at 520 nm when excited at 450 nm (B). The decay was measured by TCSPC at the indicted temperature both parallel (Ivv) and perpendicular (Ivh) to the excitation polarization, with the dye attached to the PNA and hybridized to the DNA nanocage or attached directly to the DNA nanocage. (Bottom of A and B) The anisotropy was calculated for each data point of the decay, as described in the Supporting Information, Materials and Methods section, and plotted for each complex.

anisotropy of DNA-FAM at 11 °C and at 22 °C decay to values of 0.11 and 0.12, respectively, after 17 ns. Just as with TMR, the calculated anisotropy of FAM was found to decay in nearly identical fashion regardless of whether it was attached to the PNA-peptide or directly attached to the DNA nanocage.

The steady state fluorescence spectra were measured at 11 °C for the following complexes, as shown in Figure 6: (A) the designed DNA-PNA-peptide complex (DNA + PNA1-FAM + PNA2-TMR), (B) the DNA nanocage labeled at two adjacent vertices but without any bound PNA (DNA-FAM-TMR), as well as the constructs prepared to measure PNA1-GPG thermal stability of (C) DNA-TMR + PNA1-FAM and (D) DNA-FAM + PNA1-TMR For each construct, Figure 6 shows a cartoon

dx.doi.org/10.1021/ja400762c | J. Am. Chem. Soc. 2013, 135, 6985−6993

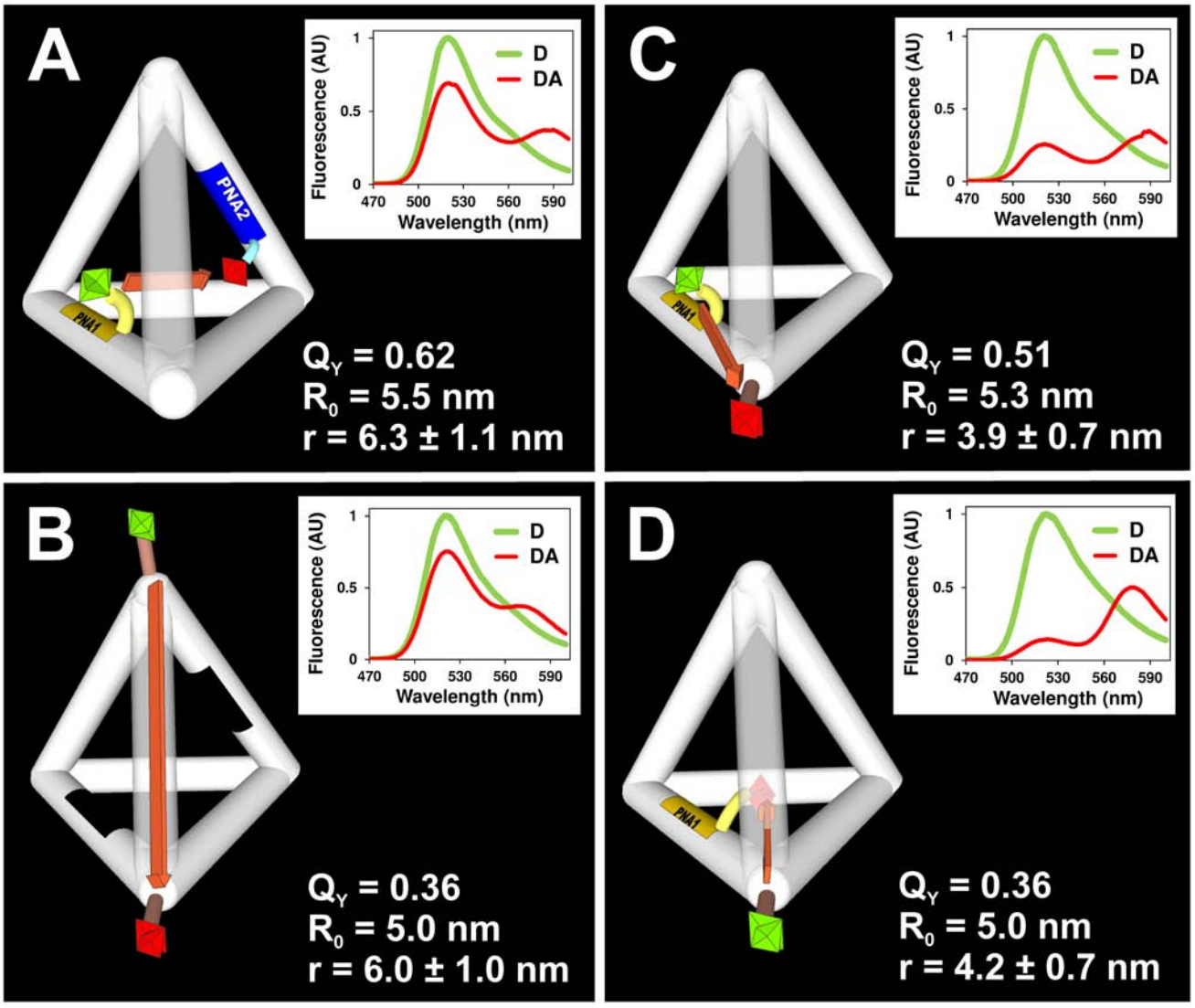

Figure 6. Förster distance measurements between FAM and TMR dyes attached to a complex of a DNA nanocage with 0, 1, or 2 PNA-peptides inside. A schematic is shown of each of the following complexes: (A) DNA + PNA1-FAM + PNA2-TMR, (B) DNA-TMR-FAM (no PNA), (C) DNA-TMR + PNA1-FAM, (D) DNA-FAM + PNA1-TMR. Next to each schematic is the fluorescence emission spectra (Ex. 450 nm) of the donor only (D) and of the donor with the acceptor (DA) measured at 11 °C along with the calculated energy transfer efficiency. Below the fluorescence spectra is the determined quantum yield (Q_Y), calculated Förster radius (R_0), and Förster distance (r).

schematic, the fluorescence spectra with the change in donor fluorescence (D) in the presence of the acceptor (DA), the determined quantum yield (Q_Y), and the calculated Förster radius (R_0) and Förster distance (r). The Q_Y of the donor only complexes were determined by comparing the fluorescence intensity of each complex (without the acceptor) to that of a sodium fluorescein standard,[41] when normalized to concentration. The calculated Q_Y for the donor (FAM) attached to the PNA1-peptide and hybridized to the DNA nanocage were higher (0.62 and 0.51) than when directly attached to the DNA nanocage vertex (0.36). This range of Q_Y were in agreement with those reported in the literature for FAM attached to dsDNA.[40,42] The change in donor (FAM) fluorescence in the presence of the acceptor (TMR) was used to determine the FRET efficiency and together with the Q_Y was used to calculate the corresponding Förster distances using the Förster equations described in the Supporting Information, Materials and Methods section. For the designed construct shown in Figure 6A, the FRET efficiency determined from steady state fluorescence (30%) is similar to the value (36%) obtained by the change in average donor lifetime observed using TCSPC.

When calculating the Förster distances, we assumed the dyes were randomly oriented, with an orientation factor (κ^2) of 2/3. However, the anisotropy data indicate that both dyes interact with the DNA nanocage, which could bias particular orientations and introduce uncertainty into the calculated distances. Dale and co-workers developed a method to determine the limits of the orientation factor based on the anisotropy data.[43] We used a variation of this method developed by Lakowicz and co-workers[44] and described in the Supporting Information, Materials and Methods section, to determine the upper and lower limits of the orientation factor (κ^2) to be between κ^2_{min} = 0.2 and κ^2_{max} = 1.7, which translates to the distance uncertainties shown in Figure 6 for each construct.

The calculated Förster distances of the different complexes in Figure 6 were used in combination with gel electrophoresis, lifetime, and anisotropy data to develop a model of the insertion and structural arrangement of the fluorescently labeled PNA-

dx.doi.org/10.1021/ja400762c | J. Am. Chem. Soc. 2013, 135, 6985−6993

peptides inside the DNA nanocage. The Förster distances of 6.3 ± 1.1 nm measured between edges through the center of the DNA nanocage (Figure 6A) and of 6.0 ± 1.0 nm measured along one of the DNA nanocage edges (Figure 6B) are slightly longer and shorter, respectively, than the corresponding distances of 7 nm and 5−6 nm, respectively, of a tetrahedron with straight edges. These measurements suggest a conformation of the DNA nanocage where the edges are bowed outward giving the tetrahedron a more spherical rather than pyramid shape, similar to a previously reported cryo-electron microscopy study.[26] The FAM labeled PNA-peptide causes a pronounced native gel band shift of the DNA nanocage upon binding, which suggests the negatively charged FAM^{2-} is repelled away from the DNA nanocage, slowing its migration through the gel. The relatively high TMR anisotropy data suggest that it strongly interacts with the DNA nanocage and stabilizes the bound PNA-peptide, resulting in a 9.2 °C increase its dissociation temperature. Gel electrophoresis data of the TMR labeled PNA-peptide show a dominant conformation that does not significantly affect the complex migration in the gel, which suggests the TMR may intercalate with the DNA nucleobases or bind on the interior of the DNA nanocage. The gel also shows minor band broadening suggesting that TMR may also nonspecifically interact with the surrounding DNA helix in a range of conformations. This TMR labeled PNA-peptide conformational heterogeneity is likely the source of the two energy transfer pathways identified using TCSPC. The donor−acceptor distances for the dominant energy pathway (2.5 ns, 36% FRET efficiency) was calculated to be 6.0 ± 1.0 nm, while the faster pathway (0.7 ns, 82% FRET efficiency) was calculated to be 4.3 ± 0.7 nm. The longer distance suggests a peptide conformation with the TMR intercalating with nearby DNA bases, while the shorter distance suggests a peptide conformation with the TMR extended into the center of the DNA nanocage toward the FAM-labeled PNA-peptide.

■ CONCLUSION

We have demonstrated a rapid and flexible method using PNA linkers to assemble peptides inside a small 3D DNA nanocage. The PNA-peptides could be introduced quantitatively by incubating for 5−10 min at room temperature with the preassembled DNA nanocage, either in parallel or stepwise fashion, with as little as two times molar excess of PNA-peptide. The TMR dye label was found to significantly stabilize PNA-peptide binding to the DNA nanocage, increasing the T_D by 9.2 °C from a predicted value of 36.6 °C to 45.8 °C. Data from biophysical characterization using gel electrophoresis as well as steady state and time-resolved fluorescence spectroscopy allowed us to develop a model for the arrangement of the PNA-peptides inside the DNA nanocage that is in agreement with the intended design.

Our design strategy can be further expanded to introduce four PNA binding gaps by shortening the length of the remaining two DNA strands (e.g., Figures S1 and S2). In order to access the remaining two edges of the DNA nanocage, two of the existing four DNA strands must each be divided into a 13bp strand and a 34bp strand, which may require further optimization of the annealing conditions for proper DNA nanocage assembly. The gaps can also be translated to other edges contacted by the same strand or shifted along the same edge to control the orientation of the N-terminally attached peptide. Additional peptides can be introduced at the C-terminus of the PNA during the initial synthesis or along the PNA backbone using orthogonal protecting groups.[45] A previous study estimated the DNA nanocage could accommodate a 60 kDa (~500 amino acid) globular protein[14] but could just as easily be filled by a series of peptides assembled together using multiple PNAs. This work illustrates how a 3D DNA scaffold can be used to assemble polypeptides through rapid and controlled hybridization with PNA linkers. The flexibility of our method offers a biomimetic route to rebuild protein active sites and further expand the structure and functional landscape of polypeptide engineering.

■ ASSOCIATED CONTENT

Supporting Information

Materials and Methods section, calculations for nucleobase and dye extinction coefficients, predicted and calculated DNA-PNA dissociation temperatures, evaluation of spectroscopic data including calculating quantum yields, fluorescence lifetimes, anisotropies, FRET efficiencies, Förster radii, and distances; supporting results and discussion on the DNA-PNA-peptide complex design and PNA-peptide synthesis; Figure S1, DNA and PNA sequences and schematic showing their arrangement in the complex; Figure S2, complex nomenclature with list of constituent DNA and PNA-peptide strand names; Figure S3, MALDI mass spectrum of the synthesized PNA-peptides; Figure S4, RP-HPLC chromatograms of the synthesized PNA-peptides; Figure S5, SE-HPLC chromatograms of the DNA nanocage with and without PNA-peptides; Figure S6, native PAGE of the DNA nanocage incubated with PNA1-GPG at 4 °C; Figure S7, chemical structures of FAM and TMR; Figure S8, absorbance of the labeled PNA1-peptide hybridized to the DNA nanocage; Figure S9, temperature dependence of FAM fluorescence; Figure S10, time course of PNA1-peptide hybridization with the DNA nanocage; Table S1, lifetime components and calculated average lifetimes of the donor and acceptor. This material is available free of charge via the Internet at http://pubs.acs.org.

■ AUTHOR INFORMATION

Corresponding Author

Petra.Fromme@asu.edu

Notes

The authors declare no competing financial interest.

■ ACKNOWLEDGMENTS

We thank Zach Laughrey and John Lopez in the ASU Protein Chemistry Lab for sharing their expertise on MALDI, peptide synthesis, and purification, as well as Anindya Roy for consultation on organic synthesis and Chad Simmons for consultation on DNA preparation and analysis. S.L. thanks Dr. Josh Holt and Dr. Andrew Ferguson of NREL for sharing the information on incorporating the Fianium laser into the TCSPC setup and for using the Fianium control software developed in their lab. This work was supported by the Center for Bio-Inspired Solar Fuel Production, an Energy Frontier Research Center funded by the U.S. Department of Energy, Office of Science, Office of Basic Energy Sciences under Award Number DE-SC0001016.

■ REFERENCES

(1) Winfree, E.; Liu, F.; Wenzler, L. A.; Seeman, N. C. *Nature* **1998**, *394*, 539−544.
(2) Goodman, R. P.; Schaap, I. A. T.; Tardin, C. F.; Erben, C. M.; Berry, R. M.; Schmidt, C. F.; Turberfield, A. J. *Science* **2005**, *310*, 1661−1665.
(3) Zheng, J.; Birktoft, J. J.; Chen, Y.; Wang, T.; Sha, R.; Constantinou, P. E.; Ginell, S. L.; Mao, C.; Seeman, N. C. *Nature* **2009**, *461*, 74−77.
(4) Shih, W.; Quispe, J.; Joyce, G. *Nature* **2004**, *427*, 618−621.

(5) Rothemund, P. W. K. *Nature* **2006**, *440*, 297−302.
(6) Douglas, S. M.; Dietz, H.; Liedl, T.; Högberg, B.; Graf, F.; Shih, W. M. *Nature* **2009**, *459*, 414−418.
(7) Aldaye, F. A.; Palmer, A. L.; Sleiman, H. F. *Science* **2008**, *321*, 1795−1799.
(8) Seeman, N. C. *Annu. Rev. Biochem.* **2010**, *79*, 65−87.
(9) Pinheiro, A. V.; Han, D.; Shih, W. M.; Yan, H. *Nat. Nanotechnol.* **2011**, *6*, 763−772.
(10) Yan, H.; Park, S. H.; Finkelstein, G.; Reif, J. H.; LaBean, T. H. *Science* **2003**, *301*, 1882−1884.
(11) Williams, B. A. R.; Lund, K.; Liu, Y.; Yan, H.; Chaput, J. C. *Angew. Chem., Int. Ed.* **2007**, *119*, 3111−3114.
(12) Wilner, O. I.; Weizmann, Y.; Gill, R.; Lioubashevski, O.; Freeman, R.; Willner, I. *Nat. Nanotechnol.* **2009**, *4*, 249−254.
(13) Umena, Y.; Kawakami, K.; Shen, J.-R.; Kamiya, N. *Nature* **2011**, *473*, 55−60.
(14) Erben, C. M.; Goodman, R. P.; Turberfield, A. J. *Angew. Chem., Int. Ed.* **2006**, *118*, 7574−7577.
(15) Pal, S.; Deng, Z.; Ding, B.; Yan, H.; Liu, Y. *Angew. Chem., Int. Ed.* **2010**, *122*, 2760−2764.
(16) Marvin Sketch was used for drawing, displaying, and characterizing chemical structures, MarvinSketch 5.11.3, 2012, ChemAxon (http://www.chemaxon.com).
(17) Nielsen, P. E.; Egholm, M.; Berg, R. H.; Buchardt, O. *Science* **1991**, *254*, 1497−1500.
(18) Fabani, M. M.; Abreu-Goodger, C.; Williams, D.; Lyons, P. A.; Torres, A. G.; Smith, K. G. C.; Enright, A. J.; Gait, M. J.; Vigorito, E. *Nucleic Acids Res.* **2010**, *38*, 4466−4475.
(19) Onyshchenko, M. I.; Gaynutdinov, T. I.; Englund, E. A.; Appella, D. H.; Neumann, R. D.; Panyutin, I. G. *Nucleic Acids Res.* **2011**, *39*, 7114−7123.
(20) Gaylord, B. S.; Massie, M. R.; Feinstein, S. C.; Bazan, G. C. *Proc. Natl. Acad. Sci. U.S.A.* **2005**, *102*, 34−39.
(21) Pokorski, J. K.; Nam, J. M.; Vega, R. A.; Mirkin, C. A.; Appella, D. H. *Chem. Commun.* **2005**, 2101−2103.
(22) Egholm, M.; Buchardt, O.; Christensen, L.; Behrens, C.; Freier, S. M.; Driver, D. A.; Berg, R. H.; Kim, S. K.; Nordcn, B.; Nielsen, P. E. *Nature* **1993**, *365*, 566−568.
(23) Demidov, V. V; Potaman, V. N.; Frank-Kamenetskii, M. D.; Egholm, M.; Buchard, O.; Sönnichsen, S. H.; Nielsen, P. E. *Biochem. Pharmacol.* **1994**, *48*, 1310−1313.
(24) Lukeman, P. S.; Mittal, A. C.; Seeman, N. C. *Chem. Commun.* **2004**, 1694−1695.
(25) Englund, E. A.; Wang, D.; Fujigaki, H.; Sakai, H.; Micklitsch, C. M.; Ghirlando, R.; Martin-Manso, G.; Pendrak, M. L.; Roberts, D. D.; Durell, S. R.; Appella, D. H. *Nat. Commun.* **2012**, *3*, 614.
(26) Kato, T.; Goodman, R. P.; Erben, C. M.; Turberfield, A. J.; Namba, K. *Nano Lett.* **2009**, *9*, 2747−2750.
(27) Wang, J. *Proc. Natl. Acad. Sci. U.S.A.* **1979**, *76*, 200−203.
(28) Rhodes, D.; Klug, A. *Nature* **1980**, *286*, 573−578.
(29) Eriksson, M.; Nielsen, P. E. *Nat. Struct. Biol.* **1996**, *3*, 410−413.
(30) Pritz, S.; Yvonne, W.; Klemm, C.; Bienert, M. *Tetrahedron Lett.* **2006**, *47*, 5893−5896.
(31) Braasch, D. A.; Nulf, C. J.; Corey, D. R. *Current Protocols in Nucleic Acid Chemistry*; John Wiley & Sons: New York, NY, 2002; pp 4.11.1−4.11.18.
(32) Lesignoli, E.; Germini, A.; Corradini, R.; Sforza, S.; Galavema, G.; Dossena, A.; Marchelli, R. *J. Chromatogr., A* **2001**, *922*, 177−185.
(33) Kuhn, H.; Demidov, V. V; Coull, J. M.; Fiandaca, M. J.; Gildea, B. D.; Frank-Kamenetskii, M. D. *J. Am. Chem. Soc.* **2002**, *124*, 1097−1103.
(34) Sahu, B.; Sacui, I.; Rapireddy, S.; Zanotti, K. J.; Bahal, R.; Armitage, B. A.; Ly, D. H. *J. Org. Chem.* **2011**, *76*, 5614−5627.
(35) Özhalici-Ünal, H.; Armitage, B. A. *ACS Nano* **2009**, *3*, 425−433.
(36) Giesen, U.; Kleider, W.; Berding, C.; Geiger, A.; Ørum, H.; Nielsen, P. E. *Nucleic Acids Res.* **1998**, *26*, 5004−5006.
(37) Wang, L.; Gaigalas, A. K.; Blasic, J.; Holden, M. J. *Spectrochim. Acta A* **2004**, *60*, 2741−2750.
(38) Sen, A.; Nielsen, P. E. *Biophys. J.* **2006**, *90*, 1329−1337.
(39) Kaji, T.; Ito, S.; Iwai, S.; Miyasaka, H. *J. Phys. Chem. B* **2009**, *113*, 13917−13925.
(40) Delgadillo, R. F.; Parkhurst, L. J. *Photochem. Photobiol.* **2010**, *86*, 261−272.
(41) Magde, D.; Wong, R.; Seybold, P. G. *Photochem. Photobiol.* **2002**, *75*, 327−334.
(42) Noble, J. E.; Wang, L.; Cole, K. D.; Gaigalas, A. K. *Biophys. Chem.* **2005**, *113*, 255−263.
(43) Dale, R. E.; Eisinger, J.; Blumberg, W. E. *Biophys. J.* **1979**, *26*, 161−193.
(44) Lakowicz, J. R.; Gryczynski, I.; Cheung, H. C.; Wang, C.-K.; Johnson, M. L.; Joshi, N. *Biochemistry* **1988**, *27*, 9149−9160.
(45) Englund, E. A.; Appella, D. H. *Angew. Chem., Int. Ed.* **2007**, *46*, 1414−1418.